https://doi.org/10.5194/gmd-2022-233
Preprint. Discussion started: 16 November 2022

Geoscientific Model Development Discussions

An Improved Parameterization of Sea Spray-Mediated Heat Flux Using Gaussian Quadrature: Case Studies with a Coupled CFSv2.0-WW3 System

Ruizi Shi[1] and Fanghua Xu[1*]

[1] Department of Earth System Science, Ministry of Education Key Laboratory for Earth System Modeling, Institute for Global Change Studies, Tsinghua University, Beijing, 100084, China.

Correspondence to: Fanghua Xu (fxu@mail.tsinghua.edu.cn)

https://doi.org/10.5194/gmd-2022-233
Preprint. Discussion started: 16 November 2022

Geoscientific Model Development Discussions

Abstract. Sea spray-mediated heat flux plays an important role in air-sea heat transfer. Heat flux integrated over droplet size spectrum can well simulate total heat flux induced by sea spray droplets. Previously, a fast spray-flux scheme assuming single-radius droplets (A15) was widely used since the full-size spectrum integral is computational expensive. Based on the Gaussian Quadrature (GQ) method, a new fast scheme (SPRAY-GQ) of sea spray-mediated heat flux is derived. The performance of SPRAY-GQ is evaluated by comparing heat fluxes with those estimated from the widely-used A15. The new scheme shows a better agreement with the original spectrum integral. To further evaluate the performance of A15 and SPRAY-GQ, the two schemes are implemented into a coupled CFSv2.0-WW3 system, and a series of 56-day simulations in summer and winter are conducted and compared. The comparisons with satellite measurements and reanalysis data show that the SPRAY-GQ scheme could simulate air-sea heat flux more reasonably than the A15 scheme. For experiments based on SPRAY-GQ, the sea surface temperature at mid-high latitudes of both hemispheres, particularly in summer, is significantly improved compared with the experiments based on A15. The simulation of 10-m wind speed and significant wave height at mid-low latitudes of the Northern Hemisphere is improved as well. The computational time of SPRAY-GQ is about the same as that of A15. Thereby, the newly-developed SPRAY-GQ scheme has a potential to be used for improving air-sea heat flux in coupled models.

https://doi.org/10.5194/gmd-2022-233
Preprint. Discussion started: 16 November 2022

Geoscientific Model Development Discussions

1 Introduction

Sea spray droplets, ejected from oceans, include film drops, jet drops and spume drops (Veron, 2015). The first two types of droplets are generated from bubble bursting caused by ocean surface wave breaking, with radius ranging from 0.5 μm to 50 μm (Resch and Afeti, 1991; Thorpe, 1992; Melville, 1996; Spiel, 1997; Andreas, 1998; Lhuissier and Villermaux, 2012). Spume drops are generated by strong winds (> 7-11 m/s) which directly tear the wave crests, with larger radius ranging from tens to hundreds μm (Koga, 1981; Andreas et al., 1995; Andreas, 1998). Sea spray droplets play an important role in weather and climate processes (Fox-Kemper et al., 2022). On one hand, sea spray droplets contribute to local marine aerosols and subsequently modify the local radiation balance (Fairall et al., 1983; Burk, 1984; Fairall and Larsen, 1984). On the other hand, sea spray droplets affect the fluxes of heat, momentum, salt, and freshwater between atmosphere and ocean (Andreas, 1992; Andreas et al., 2008; Andreas, 2010; Andreas et al., 2015; Ling and Kao, 1976; Fairall et al., 1994; Andreas and Decosmo, 2002).

The sea spray-mediated heat transfer mainly occurs within the droplet evaporation layer (DEL) near the sea surface (Andreas and Decosmo, 1999, 2002; Fairall et al., 1994). Sea spray droplets with the same temperature as ocean surface can lead to sensible heat flux in DEL, while water evaporated from these droplets can further release latent heat to the atmosphere (Andreas, 1992; Borisenkov, 1974; Bortkovskii, 1973; Wu, 1974; Monahan and Van Patten, 1988; Ling and Kao, 1976). Part of the sea spray-mediated sensible heat is absorbed by droplet evaporation, which further increases the air-sea temperature difference, and thus increases the sea spray-mediated sensible heat flux (Fairall et al., 1994; Andreas and Decosmo, 2002). Since strong winds produce more sea spray droplets with larger radius, sea spray-mediated heat fluxes increase with wind speed (Fairall et al., 1994), and contribute more than 10% of the total surface heat flux after reaching the threshold speed (> 11 m/s for sensible heat flux and > 13 m/s for latent heat flux)(Andreas et al., 2008). In addition, when a droplet is released into the air, it is accelerated due to surface winds (Edson and Andreas, 1997; Fairall et al., 1994; Van Eijk et al., 2011; Wu et al., 2017). If the droplet could fall back into the ocean, additional momentum would be injected into the ocean from the atmosphere (Andreas, 1992, 2004).

The usual bulk parameterizations in numerical models for surface fluxes only include the interfacial (turbulent) fluxes (e.g., Fairall et al., 1996), while neglecting the significant contributions of sea spray

https://doi.org/10.5194/gmd-2022-233
Preprint. Discussion started: 16 November 2022


Geoscientific Model Development Discussions

droplets in DEL (Andreas et al., 2008; Fairall et al., 1994; Smith, 1997; Emanuel, 1995). Andreas and Emanuel (2001) implemented sea spray-mediated heat flux and momentum flux parameterizations into a simple tropical cyclone model, and found that the sea spray-induced heat flux significantly enhances the tropical cyclone intensity, offsetting the negative effect of enhanced surface drag by strong wind and waves. The similar enhancement of tropical cyclone intensity was also shown in recent regional coupling systems by including sea spray-mediated heat flux (Xu et al., 2021a; Liu et al., 2012; Garg et al., 2018; Zhao et al., 2017). In the First Institute of Oceanography Earth System Model, Bao et al. (2020) first incorporated the sea spray-mediated heat flux in global climate simulation. Following Bao et al. (2020), Song et al. (2022) found the sea spray-mediated heat flux can lead to cooling at the air-sea interface and strengthening westerlies in the Southern Ocean, and thus improves estimates of sea surface temperature (SST).

Since the parameterization of sea spray-mediated heat flux derived from observations requires full-size spectral integral and demands huge amount of computational time (Andreas, 1989, 1990, 1992; Andreas et al., 2015), a simplified parameterization based on a single radius of sea spray droplets (Andreas et al., 2015; Andreas et al., 2008) is widely used in atmosphere-ocean coupling systems (Xu et al., 2021a; Liu et al., 2012; Garg et al., 2018; Zhao et al., 2017; Song et al., 2022; Bao et al., 2020), and apt to produce significant biases. To reduce biases induced by the single radius of sea spray droplets, we develop a new parameterization of sea spray-mediated heat flux based on the Gaussian Quadrature (GQ) method, a fast and accurate way to calculate spectral integral. The GQ method has been successfully used for the estimation of domain-averaged radiative flux profiles (Li and Barker, 2018). The performance of the GQ-based parameterization of the sea spray-mediated heat flux is evaluated and compared with the simplified parameterization for single radius of Andreas et al. (2015), referred to as A15 hereafter. The results are first compared with the original parameterization using full-size spectral integral (A92, hereafter). Then the parameterizations are implemented in a global coupled atmosphere-ocean-wave system (Shi et al., 2022), and the results are compared with global satellite measurements and reanalysis data.

The rest of the paper is structured as follows: observation and reanalysis data for comparisons are introduced in Section 2; the derivation of the GQ-based parameterization and the global coupling system

https://doi.org/10.5194/gmd-2022-233
Preprint. Discussion started: 16 November 2022


Geoscientific Model Development Discussions

are described in Section 3; the performance of the new parameterization is evaluated in Section 4. Finally, a summary and discussion are given in Section 5.

2 Data

The fifth generation European Centre for Medium-Range Weather Forecasts (ECMWF) Reanalysis (ERA5; Hersbach et al., 2020) data assimilated huge amounts of historical data and thus provided reliable hourly estimates. ERA5 10-m wind speed (WSP10), 2-m air temperature, 2-m dewpoint temperature, surface pressure and significant wave height (SWH) with a spatial resolution of 0.5° are used. Additionally, WSP10, 2-m air temperature and 2-m specific humidity data from the Objectively Analyzed air-sea Fluxes (OAFlux) products (Yu et al., 2008) are also applied for comparison, with 1°×1° resolution. The daily average satellite Optimum Interpolation SST (OISST) data are obtained from the National Oceanic and Atmospheric Administration (NOAA) with a spatial resolution of 0.25° (Reynolds et al., 2007). The global monthly mean salinity observation from European Space Agency (ESA; https://climate.esa.int/sites/default/files/SSS_cci-D1.1-URD-v1r4_signed-accepted.pdf) are applied.

3 Methods

3.1 Development of a Fast Algorithm Based on GQ

The effects of sea spray droplets on sensible and latent heat fluxes ($H_{S,SP}$, $H_{L,SP}$) contribute to the total sensible and latent heat fluxes ($H_{S,T}$, $H_{L,T}$) at the air-sea interface. That is,

$$H_{S,T} = H_S + H_{S,SP}, \quad (1)$$

$$H_{L,T} = H_L + H_{L,SP}. \quad (2)$$

where H_S and H_L are the sensible and latent heat fluxes at the air-sea interface due to the air-sea differences of temperature and humidity. Based on eddy correlation observations, A92 (Andreas, 1989, 1990, 1992; Andreas et al., 2015) integrates the sea spray-mediated sensible and latent heat flux spectrums over initial droplet radius ($Q_S(r_0)$ and $Q_L(r_0)$) to estimate $H_{S,SP}$ and $H_{L,SP}$ (details in Appendix A). The distributions of $Q_S(r_0)$ and $Q_L(r_0)$ spectrums as functions of initial droplet radius r_0 under various atmosphere and ocean state are shown in Fig. 1, indicating that Q_S and Q_L spectrums

https://doi.org/10.5194/gmd-2022-233
Preprint. Discussion started: 16 November 2022

Geoscientific Model Development Discussions

are more sensitive to the change of 10-m wind speed, and less sensitive to other variables, including 2-m air temperature, 2-m relative humidity, sea surface temperature, surface air pressure and sea surface salinity.

The calculation of $H_{S,SP}$ and $H_{L,SP}$ in A92 requires huge amount of computational time due to full-size spectral integral (Eqn. A5-A6 of Appendix A), therefore it is difficult to apply A92 directly in coupled modeling systems. A15 (Andreas et al., 2015) developed a fast algorithm by using a single representative droplet radius (details in Appendix B), which was widely adopted in recent reginal and global coupling systems (Xu et al., 2021a; Liu et al., 2012; Garg et al., 2018; Zhao et al., 2017; Song et al., 2022; Bao et al., 2020). In this study, we apply a 3-node GQ method (details in Appendix C) to develop a new fast algorithm to approximate the full-size spectral integral of A92. Notably, GQ can converge exponentially to the actual integral only for a smooth function (McClarren, 2018). Since as functions of r_0, Q_S and Q_L are not smooth (Fig. 1), a data sorting from largest to smallest is required. After sorting, Q_S and Q_L become Q_{SS} and Q_{LS}, and then GQ can be used to estimate the integral of Q_{SS} and Q_{LS}. However, the sorting leads to high complexity of GQ comparable to A92. Therefore, it is necessary to find the general law of GQ nodes for Q_{SS} and Q_{LS} to avoid the sorting in application.

To derive the general law of GQ nodes, we calculate the distribution of the sea spray-mediated heat flux spectral following A92, based on the global daily WSP10, 2-m air temperature, 2-m dewpoint temperature, surface pressure and SWH of ERA5 and OISST from August 1, 2018 to August 31, 2018. The ESA monthly salinity is also applied since the sea spray-mediated heat flux is the least sensitive to salinity (Fig. 1e&f) and only monthly salinity observation data is available. From the global spectrums, we sort Q_S and Q_L from largest to smallest. The GQ nodes corresponding to r_0 of the sensible (latent) heat flux after sorting are denoted as r_{S1}, r_{S2} and r_{S3} (r_{L1}, r_{L2} and r_{L3}), whose distribution of occurrence frequency in percentage is shown in Fig. 2. It is noted that except that r_{L3} is related to WSP10 (Fig. 2c), all other five nodes have frequency roughly concentrated at a constant (peak frequency >65%), that is

$$r_{S1} = 459.056,\ r_{S2} = 294.185,\ r_{S3} = 166.771, \quad (3)$$

$$r_{L1} = 443.914, r_{L2} = 251.0498, \quad (4)$$

https://doi.org/10.5194/gmd-2022-233
Preprint. Discussion started: 16 November 2022

Geoscientific Model Development Discussions

$$r_{L3} = \begin{cases} 60.310\mathrm{WSP10}^{0.1161}, & \mathrm{WSP10} \geq 2\ m/s \\ 58.086, & \mathrm{WSP10} < 2\ m/s \end{cases}, \quad (5)$$

where the unit of the radius is micrometer. And then the 3-node GQ to approximate the full-size spectral integral of A92 are

$$\int_a^b Q_S(r_0)dr_0 \approx \frac{b-a}{2}\sum_{i=1}^{3}\omega_i Q_S(r_{Si}), \quad (6)$$

$$\int_a^b Q_L(r_0)dr_0 \approx \frac{b-a}{2}\sum_{i=1}^{3}\omega_i Q_L(r_{Li}). \quad (7)$$

Here a and b are the lower and upper limits of r_0, which are set to $2\mu m$ and $500\mu m$ based on Andreas (1990), and ω_i is the corresponding weight (ω_1=ω_3=0.556, ω_2=0.889), obtained from McClarren (2018). Thus, we can directly use Eqn. (3-7) to estimate the GQ-based $H_{S,SP}$ and $H_{L,SP}$ approximations, avoiding sorting. The new fast algorithm is referred to as SPRAY-GQ hereafter.

3.2 CFSv2.0-WW3 Coupling System

A coupled system based on Climate Forecast System model version 2.0 (CFSv2.0) and WAVEWATCH III (WW3) is employed to evaluate and compare the effects of sea spray-mediated heat flux parameterized by A15 and SPRAY-GQ. The CFSv2.0-WW3 has three components, the Global Forecast System (GFS; http://www.emc.ncep.noaa.gov/GFS/doc.php) as the atmosphere component of CFSv2.0, the Modular Ocean Model version 4 (MOM4; Griffies et al., 2004) as the ocean component of CFSv2.0, and the WW3 (WAVEWATCH III Development Group, 2016) as the ocean surface wave component. The variables between CFSv2.0 and WW3 are interpolated and passed using the Chinese Community Coupler version 2.0 (C-Coupler2; Liu et al., 2018).

The CFSv2.0 is mainly applied for intraseasonal and seasonal prediction (e.g., Saha et al., 2014). The atmosphere component GFS uses a spectral triangular truncation of 382 waves (T382) in the horizontal, equivalent to a grid resolution of nearly 35 km, and 64 sigma-pressure hybrid layers in the vertical. The MOM4 is integrated on a nominal 0.5° horizontal grid with enhanced horizontal resolution to 0.25° in the tropics, and there are 40 levels in the vertical. The latitude range of WW3 is 78°S–78°N with a spatial resolution of 1/3°. In the coupling system, the WW3 obtains 10-m wind and ocean surface current from CFSv2.0, and then provides wave parameters to CFSv2.0. Several wave-mediated processes, including

https://doi.org/10.5194/gmd-2022-233
Preprint. Discussion started: 16 November 2022


Geoscientific Model Development Discussions

upper ocean mixing modified by Stokes drift-related processes, air-sea fluxes modified by surface current and Stokes drift, and momentum roughness length, are considered. Details of this system are referred to Shi et al. (2022).

A series of numerical experiments is conducted to evaluate the effects of the two parameterizations (A15 and SPRAY-GQ) of sea spray-mediated heat flux on ocean, atmosphere and waves in two 56-day periods, from January 3 to February 28, 2017 and from August 3 to September 28, 2018 for boreal winter and boreal summer, respectively. For each period, two sensitivity experiments are carried out. The first is the SPRAY-A15 experiment, in which A15 is used with two-way fully coupling. The second is the SPRAY-GQ experiment, in which SPRAY-GQ parameterization is used instead of A15.

4 Results

4.1 Comparison with A92

Based on the daily global WSP10, 2-m air temperature, 2-m dewpoint temperature, surface pressure and SWH of ERA5, the daily global OISST, and the ESA monthly global salinity, $H_{S,SP}$ and $H_{L,SP}$ from A15, SPRAY-GQ and A92 are calculated (Fig. 3). The computational time for SPRAY-GQ is about the same as that for A15, and about 36 times less than the time for A92. Compared with A92 (the black dotted line), A15 (red) overestimates $H_{S,SP}$ for low $H_{S,SP}$ (<50 W/m^2) and underestimates $H_{S,SP}$ for high $H_{S,SP}$ (>50 W/m^2) with a root mean square error (RMSE) of 3.40 W/m^2 (Fig. 3a), while A15 shows consistent overestimations with a RMSE of 2.98 W/m^2 for $H_{L,SP}$ (Fig. 3b). Overall, the RMSE of A15 is about 2.69 W/m^2 for sea-spray mediated total heat flux ($TH_{SP} = H_{S,SP}+H_{L,SP}$; Fig. 3c). Compared with A15, SPRAY-GQ (blue) has less deviation from A92 for both $H_{S,SP}$ and $H_{L,SP}$ (Fig. 3a&b). The corresponding RMSEs of SPRAY-GQ for $H_{S,SP}$, $H_{L,SP}$ and TH_{SP} are 0.83 W/m^2, 0.92 W/m^2 and 0.62 W/m^2, all significantly lower (P<0.05 in Student's t-test) than those of A15.

To test robustness of the results, we also use WSP10, 2-m air temperature and 2-m specific humidity of OAFlux dataset to estimate $H_{S,SP}$ and $H_{L,SP}$. As shown in Fig. 4, SPRAY-GQ has significantly (P<0.05 in Student's t-test) lower deviations and RMSEs than A15, consistent with Fig. 3. Note that the values of $H_{S,SP}$ and $H_{L,SP}$ in Fig.4 are larger than those in Fig. 3, since the equivalent neutral wind

https://doi.org/10.5194/gmd-2022-233
Preprint. Discussion started: 16 November 2022


Geoscientific Model Development Discussions

speed from OAFlux is generally overestimated compared to the observed wind speed (Seethala et al., 2021; Praveen Kumar et al., 2012). In addition, since it is common to derive SWH from empirical equations (e.g., Andreas et al., 2008; Andreas et al., 2015; Andreas and Decosmo, 2002; Andreas, 1992), we also use SWH generated by empirical equations of WSP10 (Andreas, 1992) instead of ERA5 SWH to estimate $H_{S,SP}$ and $H_{L,SP}$ (Fig. 5). Again, the RMSEs decrease significantly (P<0.05 in Student's t-test) in SPRAY-GQ compared to A15, though the RMSEs become higher for all estimates due to the enhanced biases of SWH. Thereby, it is clear that the performance of SPRAY-GQ is always better than A15. Next, we will evaluate and compare the two fast algorithms in an atmosphere-ocean-wave coupled system (CFSv2.0-WW3).

4.2 Comparison in the CFSv2.0-WW3 Coupling System

In this section, comparisons are made for simulated SSTs, WSP10s as well as SWHs against OISST and ERA5 reanalysis (Figs. 6-11). The results in the first three days are excluded in the comparison, since the wave influences are weak at the beginning of the simulations. The computational time is about the same for experiments SPRAY-GQ and SPRAY-A15.

4.2.1 Sea Surface Temperature (SST)

In the austral summer, compared with OISST, large SST biases (>1 ℃ or <-1 ℃) of SPRAY-A15 occur in the Southern Hemisphere (SH; Fig. S1a in supplementary), especially in the Southern Ocean. It is always a challenge for reducing the large SST biases in the Southern Ocean for climate models (e.g., Alessandro et al., 2019; Wang et al., 2014; Li et al., 2013; Bodas-Salcedo et al., 2012; Ceppi et al., 2012). In Fig. 6a, SSTs north (south) of 50°S in experiment SPRAY-A15 are mainly underestimated (overestimated). The domain-averaged RMSE (0-360°E, 40-75°S) increases in the first month and then levels off (red line in Fig. 6c). While the domain-averaged RMSE in experiment SPRAY-GQ levels off about a week earlier (black line in Fig. 6c). The time series of RMSE in SPRAY-GQ is significantly lower than that in SPRAY-A15 (P<0.05 in Student's t-test). The decreased SST RMSE in SPRAY-GQ is resulted from the increased (decreased) SSTs north (south) of 50°S (Fig. 6b).

To understand the effects of sea spray droplets on SST, we calculate the total heat flux (TH=$H_{S,T}$+$H_{L,T}$)

https://doi.org/10.5194/gmd-2022-233
Preprint. Discussion started: 16 November 2022

Geoscientific Model Development Discussions

differences between SPRAY-GQ and SPRAY-A15 (Fig. 12g). The TH differences are significantly correlated with SST differences (Fig. S1b in the supplementary), with the spatial correlation coefficient of -0.41 ($P<0.05$ in Student's t-test). We further decompose direct and indirect effects of sea spray droplets on heat fluxes following Song et al. (2022). The direct effect ($H_{S,SP}$ and $H_{L,SP}$) is induced directly by sea spray droplets, calculated from A15 (Eqn. B1-B4 of Appendix B) and SPRAY-GQ (Section 3.1). The indirect effect (H_S and H_L) is the heat flux variation induced by changes of atmosphere and ocean variables (including wind, pressure, humidity and temperature) caused by direct effect, estimated by subtracting $H_{S,SP}$ and $H_{L,SP}$ from the output heat fluxes ($H_{S,T}$ and $H_{L,T}$) of experiment SPRAY-A15 and SPRAY-GQ.

In the Southern Ocean, although direct differences of $H_{S,SP}$ and $H_{L,SP}$ are relatively small (<10 W/m^2, Fig. 12b, e, &h), the resulting changes of temperature and humidity lead to relatively large differences in indirect effects of H_S and H_L (Fig. 12c, f, &i). Enhanced (reduced) $TH_{S,SP}$ from ocean to atmosphere in the summer leads to increased (decreased) air-sea temperature difference and thus enhances (weakens) H_S. Meanwhile the warmer (cooler) air also causes more (less) evaporation and thus more (less) H_L. Finally, the enhanced (reduced) TH cools (warms) SST.

In the boreal summer, large SST biases (>1 ℃ or <-1 ℃) of SPRAY-A15 mainly occur at mid-high latitudes of the Northern Hemisphere (NH; Fig. S2a in supplementary). Significant underestimations occur in the western and northern part of the North Pacific and at mid latitudes of the North Atlantic, while large positive SST biases mainly occur in the eastern part of the North Pacific and at high latitudes of the North Atlantic (Fig. 7a). In experiment SPRAY-GQ, SSTs are warmer (cooler) in the previously underestimated (overestimated) regions (Fig. 7b). Therefore, the domain-averaged RMSE (0-360°E, 20-75°N) in SPRAY-GQ is significantly lower ($P<0.01$ in Student's t-test) than in SPRAY-A15 after the first three weeks (Fig. 7c). The spatial correlation coefficient between TH differences and SST differences (Fig. 13g&Fig. S2b) is -0.32 ($P<0.05$ in Student's t-test). Consistent with the austral summer, the SST changes are related to the changes of heat flux (Fig. 13). The indirect effects of latent heat flux (Fig. 13c) play a major role in TH differences, which are modified by the direct effects (Fig. 13b, e, &h). In addition, the changes of surface wind also contribute to the changes of SST. The enhanced (reduced) winds lead to stronger (weaker) ocean mixing, and thus cooler (warmer) SST (Fig. S3&S4).

https://doi.org/10.5194/gmd-2022-233
Preprint. Discussion started: 16 November 2022


Geoscientific Model Development Discussions

4.2.2 10-m Wind Speed (WSP10) and Significant Wave Height (SWH)

Compared with experiment SPRAY-A15, significant improvements of WSP10 in SPRAY-GQ occur at mid-low latitudes of the NH (0-360°E, 0-60°N) in both winter and summer (Fig.8&9). The domain-averaged bias of WSP10 (SPRAY-A15 minus ERA5) is 0.37 m/s and 0.24 m/s in winter and summer, respectively, mainly due to the overestimations over the Pacific and the Atlantic Ocean (red in Fig.8a&9a). Whereas in SPRAY-GQ, the domain-averaged bias (SPRAY-GQ minus ERA5) is 0.26 m/s and 0.03 m/s in winter and summer respectively. The domain-averaged RMSEs of WSP10s increase with time in the first two weeks and then gradually level off (Fig. 8c&9c). The differences of WSP10 RMSEs between SPRAY-GQ (black) and SPRAY-A15 (red) are very small in the first two weeks. Afterwards the time series of RMSE in SPRAY-GQ is lower than that in SPRAY-A15 significantly at 99% confidence level in both boreal winter (Fig. 8c) and boreal summer (Fig. 9c).

The simulated SWHs changes are closely related to the changes of WSP10 (Shi et al. 2022). Therefore, the differences of SWHs (Fig.10&11) are consistent with those of WSP10s (Fig.8&9), with overestimated (underestimated) WSP10s corresponding to overestimated (underestimated) SWHs compared with ERA5. The SWHs in SPRAY-GQ improve compared with those in SPRAY-A15 (Fig. 10b&11b). In winter (summer), the SWH RMSE averages for SPRAY-A15 and SPRAY-GQ are 1.31 m (0.98 m) and 1.23 m (0.87 m), and after the first two weeks the time series of RMSE in SPRAY-GQ is lower than that in SPRAY-A15 significantly at 99% confidence level in both winter (Fig. 10c) and summer (Fig. 11c).

The direct and indirect effects of sea spray droplets on heat fluxes can influence estimates of WSP10 and then SWH. The changes of WSP10s are related to the direct effects ($H_{S,SP}$ and $H_{L,SP}$; Fig. 12b, e, &h; Fig. 13b, e, &h). The spatial correlation coefficients between WSP10 differences (Fig. S3b&S4b) and TH_{SP} differences (Fig. 12h&13h) are 0.51 and 0.69 ($P<0.01$ in Student's t-test) in winter and summer, respectively. Because the directly increased (decreased) heat fluxes enhance (reduce) turbulence, promote (hinder) the downward transmission of momentum from the upper layer of atmosphere, and then accelerate (decelerate) the surface wind speed (Wallace et al., 1989). While the accelerated (decelerated) WSP10s further result in increased (decreased) interfacial heat transport (H_S, H_L), as well as increased (decreased) SWHs.

https://doi.org/10.5194/gmd-2022-233
Preprint. Discussion started: 16 November 2022

Geoscientific Model Development Discussions

5 Conclusions and Discussions

Based on a GQ method, we develop a new fast algorithm based on Andreas's (1989, 1990, 1992) full-size microphysical parameterization (A92) for sea spray-mediated heat fluxes. Using global satellite measurements and reanalysis data, SPRAY-GQ parameterization is validated to approximate A92 more accurately than the A15 fast algorithm (Andreas et al., 2015). To evaluate the SPRAY-GQ/A15 parameterization, we implement them in the two-way coupled CFSv2.0-WW3 system. A series of 56-day simulations from January 3 to February 28, 2017 and from August 3 to September 28, 2018 are conducted. The results are compared against OISST satellite measurements and ERA5 reanalysis. The comparison shows that the sea spray-mediated heat flux in SPRAY-GQ can reasonably modulate total heat flux, significantly improve the SST biases in the Southern Ocean (mid-high latitudes of the NH) for the austral (boreal) summer, as well as WSP10 and SWH at mid-low latitudes of the NH for both boreal winter and summer. Overall, our fast algorithm based on GQ is applicable to sea spray-mediated heat flux parameterization in coupled models.

In addition to the variables aforementioned, the changes of simulated cloud fraction were also compared. However, the effects of sea spray-mediated heat flux on cloud fraction are non-significant for the 2-month simulation, so the results are not shown. Besides, for simulated WSP10 and SWH, the SPRAY-GQ parameterization used in the study mainly improves the biases at mid-low latitudes of the NH, while the significant overestimations in the SH are only slightly improved (Fig. S3-S6 in supplementary). As Andreas (2004) indicated, sea spray droplets also influence the surface momentum flux by injecting more momentum into the ocean from the atmosphere, which might further decrease the surface wind speed. We will consider this process in the future study.

Sea spray-mediated heat fluxes are sensitive to the sea spray generation function dF/dr_0. Based on a number of laboratory and field observations, varieties of dF/dr_0 were derived (e.g., Koga, 1981; Monahan et al., 1982; Troitskaya et al., 2018; Andreas, 1992, 1998, 2002; Fairall et al., 1994; Veron, 2015), whereas their differences can reach six orders of magnitude (Andreas, 1998). There is currently no consensus on the most suitable choice. In this study, we use dF/dr_0 of Fairall et al. (1994), recommended by Andreas (2002). It is also consistent with recent observations of Xu et al. (2021b). Since the new scheme based on GQ is independent of sea spray generation function, the new scheme can

https://doi.org/10.5194/gmd-2022-233
Preprint. Discussion started: 16 November 2022

Geoscientific Model Development Discussions

also be applied to sea spray-mediated heat fluxes estimation with different dF/dr_0.

Appendix A

Microphysical Parameterization of A92

Based on the cloud microphysical parameterization of Pruppacher and Klett (1978), Andreas (1989, 1990, 1992) proposed a parameterization of sea spray-related heat fluxes for droplets with different radius, from formation at sea surface to equilibrium with environment, that is,

$$Q_S = \rho_w C_{ps}(T_w - T_{eq})\left[1 - \exp\left(-\frac{\tau_f}{\tau_T}\right)\right]\left(\frac{4\pi r_0^3}{3}\frac{dF}{dr_0}\right), \quad \text{(A1)}$$

$$Q_L = \begin{cases} \rho_w L_v\left\{1 - [\frac{r(\tau_f)}{r_0}]^3\right\}\left(\frac{4\pi r_0^3}{3}\frac{dF}{dr_0}\right), \tau_f \le \tau_r, \\ \rho_w L_v\left\{1 - (\frac{r_{eq}}{r_0})^3\right\}\left(\frac{4\pi r_0^3}{3}\frac{dF}{dr_0}\right), \tau_f > \tau_r. \end{cases} \quad \text{(A2)}$$

Here Q_S, Q_L are sensible heat flux and latent heat flux resulted by sea spray droplets with initial radius r_0, ρ_w is the sea water density, C_{ps} is the specific heat, L_v is the latent heat of vaporization of water, T_w is the water temperature, T_{eq} is the temperature of droplet when it reaches thermal equilibrium with ambient condition, r_{eq} is the radius of droplet when it reaches moisture equilibrium with ambient condition, τ_f is the residence time for droplets in the atmospheric, $r(\tau_f)$ is the corresponding radius, τ_T is the characteristic e-folding time of droplet temperature, and τ_r is the characteristic e-folding time of droplet radius. The detailed calculation of these microphysical quantities can be found in Andreas (1989, 1990, 1992). And dF/dr_0 is the sea spray generation function, which represents the number produced of droplets with initial radius r_0 (Andreas, 1992). For this term, the function of Fairall et al. (1994) was recommended by Andreas (2002). According to the review in Andreas (2002), the dF/dr_0 of Fairall et al. (1994) is related on that of Andreas (1992) as

$$\frac{dF}{dr_0} = 38 \times 3.84 \times 10^{-6} U_{10}^{3.41} r_0^{-0.024} \left.\frac{dF_{A92}}{dr_{80}}\right|_{U_{10}=11\ m/s}, \quad \text{(A3)}$$

$$\left.\frac{dF_{A92}}{dr_{80}}\right|_{U_{10}=11\ m/s} = \begin{cases} e^{(4.405-2.646(logr_{80})-3.156(logr_{80})^2+8.902(logr_{80})^3-4.482(logr_{80})^4)}, r_{80} \le 15\mu m; \\ 1.02\times10^4 r_{80}^{-1}, 15 \le r_{80} \le 37.5\mu m; \\ 6.95\times10^6 r_{80}^{-2.8}, 37.5 \le r_{80} \le 100\mu m; \\ 1.75\times10^{17} r_{80}^{-8}, r_{80} \ge 100\mu m \end{cases}. \quad \text{(A4)}$$

Here U_{10} is the 10-m wind, $r_{80} = 0.518 r_0^{0.976}$.

https://doi.org/10.5194/gmd-2022-233
Preprint. Discussion started: 16 November 2022

Geoscientific Model Development Discussions

306 The total sea spray fluxes are obtained by integrating Q_S and Q_L corresponding to all r_0. Based on
307 Andreas (1990), the lower and upper limits of r_0 is $2\mu m$ and $500\mu m$, that is,

$$\overline{Q_S} = \int_2^{500} Q_S(r_0)dr, \quad \text{(A5)}$$

$$\overline{Q_L} = \int_2^{500} Q_L(r_0)dr. \quad \text{(A6)}$$

308 While $\overline{Q_S}$ and $\overline{Q_L}$ are nominal sea spray fluxes but not the actual $H_{S,SP}$ and $H_{L,SP}$ (Andreas and
309 Decosmo, 1999, 2002), because there are interactions between these two terms and the microphysical
310 functions also lead to uncertainties (Fairall et al., 1994). Therefore, $\overline{Q_S}$ and $\overline{Q_L}$ are tuned by non-
311 negative constants α, β and γ (Andreas and Decosmo, 2002; Andreas et al., 2008; Andreas et al., 2015;
312 Andreas, 2003) as

$$H_{S,SP} = \beta\overline{Q_S} - (\alpha - \gamma)\overline{Q_L}, \quad \text{(A7)}$$

$$H_{L,SP} = \alpha\overline{Q_L}. \quad \text{(A8)}$$

313 In Eqn. (A8), the α term indicates the sea spray-mediated latent heat flux from the top of DEL to
314 atmosphere. Because the evaporation of droplets absorbs heat, which is provided by sea spray-mediated
315 sensible heat (Fairall et al., 1994), the negative α term appears in Eqn. (A7). Whereas the evaporation
316 also cools DEL and thus increases the air-sea temperature difference, therefore it contributes to a positive
317 γ term in Eqn. (A7). Different values of α, β and γ were given in Andreas and Decosmo (2002),
318 Andreas (2003), Andreas et al. (2008) and Andreas et al. (2015), to minimize the bias between
319 estimations and observations of turbulent heat fluxes measured by eddy correlation. And Andreas et al.
320 (2015) validated the most observation data, which are 4000 sets, to derive $\alpha = 2.46, \beta = 15.15, \gamma =$
321 1.77.

322 **Appendix B**

323 **Fast Algorithm of A15**

324 Andreas (2003) and Andreas et al. (2008, 2015) developed a fast algorithm to approximate $H_{S,SP}$,
325 $H_{L,SP}$ by a characteristic radius, that is,

$$H_{S,SP} = \beta\overline{Q_S} - (\alpha - \gamma)\overline{Q_L} \approx \rho_w C_{ps}(T_W - T_{eq,100})V_s(u_*), \quad \text{(B1)}$$

$$H_{L,SP} = \alpha\overline{Q_L} \approx \rho_w L_v \left\{1 - [\frac{r(\tau_{f,50})}{50\mu m}]^3\right\} V_L(u_*). \quad \text{(B2)}$$

https://doi.org/10.5194/gmd-2022-233
Preprint. Discussion started: 16 November 2022

Geoscientific Model Development Discussions

Here $T_{eq,100}$ is T_{eq} of droplets with r_0=100 μm, $\tau_{f,50}$ is τ_f of droplets with r_0=50 μm, V_s and V_L are functions of the bulk friction velocity u_*. As indicated by Andreas et al. (2008, 2015), the characteristic radiuses of 100 μm and 50 μm for sensible and latent heat fluxes are chosen, respectively, because Q_S and Q_L show a large peak in the vicinity of these values (Fig. 1). V_s and V_L are calculated in Andreas et al. (2015) as

$$V_S = \begin{cases} 3.92 \times 10^{-8}, & 0 \le u_* \le 0.1480\ m/s \\ 5.02 \times 10^{-6} u_*^{2.54}, & u_* \ge 0.1480\ m/s \end{cases}, \tag{B3}$$

$$V_L = \begin{cases} 1.76 \times 10^{-9}, & 0 \le u_* \le 0.1358\ m/s \\ 2.08 \times 10^{-7} u_*^{2.39}, & u_* \ge 0.1358\ m/s \end{cases}. \tag{B4}$$

Appendix C

Gaussian Quadrature (GQ)

GQ is a method to approximate the definite integral of a function $f(x)$ via the function values at a small number of specified nodes (Gauss, 1815; Jacobi, 1826). In this study we use the form of n-node Gauss–Legendre quadrature on [-1, 1] as

$$\int_{-1}^{1} f(x)dx \approx \sum_{i=1}^{n} \omega_i f(x_i). \tag{C1}$$

Here x_i is the specified node, and ω_i is the corresponding weight. For n=3, x_1=-0.775, x_2=0, x_3=0.775, ω_1=ω_3=0.556, ω_2=0.889.

While for a function $g(\xi)$ on [a, b], Eqn. (C1) can be transformed to

$$\begin{aligned} \int_a^b g(\xi)d\xi &= \int_{-1}^{1} g\left(\frac{b-a}{2}x + \frac{a+b}{2}\right)\frac{d\xi}{dx}dx \\ &\approx \frac{b-a}{2}\sum_{i=1}^{n} \omega_i g\left(\frac{b-a}{2}x_i + \frac{a+b}{2}\right). \end{aligned} \tag{C2}$$

Code and data availability

The code of sea spray can be found under https://doi.org/10.5281/zenodo.7100345 (Shi and Xu, 2022). The code for CFSv2.0-WW3 system can be found under https://doi.org/10.5281/zenodo.5811002 (Shi et al., 2021) including the coupling, preprocessing, run control and postprocessing scripts. The initial fields for CFSv2.0 are generated by the real time operational Climate Data Assimilation System, downloaded from the CFSv2.0 official website (http://nomads.ncep.noaa.gov/pub/data/nccf/com/cfs/prod). The daily

https://doi.org/10.5194/gmd-2022-233
Preprint. Discussion started: 16 November 2022


Geoscientific Model Development Discussions

345 average satellite Optimum Interpolation SST (OISST) data are obtained from NOAA
346 (https://www.ncdc.noaa.gov/oisst). The fifth generation European Centre for Medium-Range Weather
347 Forecasts (ECMWF) Reanalysis (ERA5) are available at the Copernicus Climate Change Service (C3S)
348 Climate Date Store (https://cds.climate.copernicus.eu/cdsapp#!/dataset/reanalysis-era5-single-levels).
349 The daily Objectively Analyzed air-sea Fluxes (OAFlux) products are available at
350 https://oaflux.whoi.edu/heat-flux. The global monthly mean salinity observation of European Space
351 Agency (ESA) are from https://climate.esa.int.

352 **Author contribution**

353 FX and RS designed the experiments and RS carried them out. RS developed the code of coupling
354 parametrizations and produced the figures. RS prepared the manuscript with contributions from all co-
355 authors. FX contributed to review and editing.

356 **Acknowledgments**

357 This work was supported by the National Key Research and Development Program of China
358 (2020YFA0607900, 2021YFC3101601), and the National Natural Science Foundation of China
359 (42176019). We also thank Dr. Jiangnan Li for help of GQ codes.

360 **Competing Interests**

361 The contact author has declared that neither they nor their co-authors have any competing interests.

362 **References**

363 Alessandro, J. D., Diao, M., Wu, C., Liu, X., Jensen, J. B., and Stephens, B. B.: Cloud phase and relative
364 humidity distributions over the Southern Ocean in austral summer based on in situ observations and
365 CAM5 simulations, Journal of Climate, 32, 2781-2805, 2019.
366 Andreas, E. L.: Thermal and size evolution of sea spray droplets, 1989.
367 Andreas, E. L.: Time constants for the evolution of sea spray droplets, Tellus B, 42, 481-497, 1990.
368 Andreas, E. L.: Sea spray and the turbulent air‐sea heat fluxes, Journal of Geophysical Research:

https://doi.org/10.5194/gmd-2022-233
Preprint. Discussion started: 16 November 2022

369 Oceans, 97, 11429-11441, 1992.
370 Andreas, E. L., Edson, J. B., Monahan, E. C., Rouault, M. P., and Smith, S. D.: The spray contribution
371 to net evaporation from the sea: A review of recent progress, Boundary-Layer Meteorology, 72, 3-52,
372 1995.
373 Andreas, E. L.: A new sea spray generation function for wind speeds up to 32 ms− 1, Journal of Physical
374 Oceanography, 28, 2175-2184, 1998.
375 Andreas, E. L., and Decosmo, J.: Sea spray production and influence on air-sea heat and moisture fluxes
376 over the open ocean, in: Air-sea exchange: physics, chemistry and dynamics, Springer, 327-362, 1999.
377 Andreas, E. L., and Emanuel, K. A.: Effects of sea spray on tropical cyclone intensity, Journal of the
378 atmospheric sciences, 58, 3741-3751, 2001.
379 Andreas, E. L.: A review of the sea spray generation function for the open ocean, Advances in Fluid
380 Mechanics, 33, 1-46, 2002.
381 Andreas, E. L., and Decosmo, J.: The signature of sea spray in the HEXOS turbulent heat flux data,
382 Boundary-layer meteorology, 103, 303-333, 2002.
383 Andreas, E. L.: 3.4 AN ALGORITHM TO PREDICT THE TURBULENT AIR-SEA FLUXES IN
384 HIGH-WIND, SPRAY CONDITIONS, 2003.
385 Andreas, E. L.: Spray stress revisited, Journal of physical oceanography, 34, 1429-1440, 2004.
386 Andreas, E. L., Persson, P. O. G., and Hare, J. E.: A bulk turbulent air–sea flux algorithm for high-wind,
387 spray conditions, Journal of Physical Oceanography, 38, 1581-1596, 2008.
388 Andreas, E. L.: Spray-mediated enthalpy flux to the atmosphere and salt flux to the ocean in high winds,
389 Journal of physical oceanography, 40, 608-619, 2010.
390 Andreas, E. L., Mahrt, L., and Vickers, D.: An improved bulk air – sea surface flux algorithm, including
391 spray - mediated transfer, Quarterly Journal of the Royal Meteorological Society, 141, 642-654, 2015.
392 Bao, Y., Song, Z., and Qiao, F.: FIO - ESM version 2.0: Model description and evaluation, Journal of
393 Geophysical Research: Oceans, 125, e2019JC016036, 2020.
394 Bodas-Salcedo, A., Williams, K., Field, P., and Lock, A.: The surface downwelling solar radiation
395 surplus over the Southern Ocean in the Met Office model: The role of midlatitude cyclone clouds, Journal
396 of Climate, 25, 7467-7486, 2012.

https://doi.org/10.5194/gmd-2022-233
Preprint. Discussion started: 16 November 2022

Geoscientific Model Development Discussions

397 Borisenkov, E.: Some mechanisms of atmosphere-ocean interaction under stormy weather conditions,
398 Probl Arct Antarct, 43, 73-83, 1974.
399 Bortkovskii, R.: On the mechanism of interaction between the ocean and the atmosphere during a storm,
400 Fluid Mech Sov Res, 2, 87-94, 1973.
401 Burk, S. D.: The generation, turbulent transfer and deposition of the sea-salt aerosol, Journal of
402 Atmospheric Sciences, 41, 3040-3051, 1984.
403 Ceppi, P., Hwang, Y. T., Frierson, D. M., and Hartmann, D. L.: Southern Hemisphere jet latitude biases
404 in CMIP5 models linked to shortwave cloud forcing, Geophysical Research Letters, 39, 2012.
405 Edson, J. B., and Andreas, E. L.: Modeling the role of sea spray on air-sea heat and moisture exchange,
406 Final Rep, 6, 18, 1997.
407 Emanuel, K. A.: Sensitivity of tropical cyclones to surface exchange coefficients and a revised steady-
408 state model incorporating eye dynamics, Journal of Atmospheric Sciences, 52, 3969-3976, 1995.
409 Fairall, C., Davidson, K., and Schacher, G.: An analysis of the surface production of sea ‐ salt aerosols,
410 Tellus B, 35, 31-39, 1983.
411 Fairall, C., and Larsen, S. E.: Dry deposition, surface production and dynamics of aerosols in the marine
412 boundary layer, Atmospheric Environment (1967), 18, 69-77, 1984.
413 Fairall, C., Kepert, J., and Holland, G.: The effect of sea spray on surface energy transports over the
414 ocean, Global Atmos. Ocean Syst, 2, 121-142, 1994.
415 Fairall, C., Bradley, E. F., Rogers, D. P., Edson, J. B., and Young, G. S.: Bulk parameterization of air ‐
416 sea fluxes for tropical ocean ‐ global atmosphere coupled ‐ ocean atmosphere response experiment,
417 Journal of Geophysical Research: Oceans, 101, 3747-3764, 1996.
418 Fox-Kemper, B., Johnson, L., and Qiao, F.: Ocean near-surface layers, in: Ocean Mixing, Elsevier, 65-
419 94, 2022.
420 Garg, N., Ng, E. Y. K., and Narasimalu, S.: The effects of sea spray and atmosphere–wave coupling on
421 air–sea exchange during a tropical cyclone, Atmospheric Chemistry and Physics, 18, 6001-6021, 2018.
422 Gauss, C. F.: Methodvs nova integralivm valores per approximationem inveniendi, apvd Henricvm
423 Dieterich, 1815.
424 Griffies, S. M., Harrison, M. J., Pacanowski, R. C., and Rosati, A.: A technical guide to MOM4, GFDL

https://doi.org/10.5194/gmd-2022-233
Preprint. Discussion started: 16 November 2022

425 Ocean Group Tech. Rep, 5, 342, 2004.

426 WAVEWATCH III Development Group: User manual and system documentation of WAVEWATCH
427 III version 5.16, NOAA/NWS/NCEP/MMAB Technical Note 329, 326, 2016.

428 Hersbach, H., Bell, B., Berrisford, P., Hirahara, S., Horányi, A., Muñoz‐Sabater, J., Nicolas, J., Peubey,
429 C., Radu, R., and Schepers, D.: The ERA5 global reanalysis, Quarterly Journal of the Royal
430 Meteorological Society, 146, 1999-2049, 2020.

431 Jacobi, C. G. J.: Ueber Gauss neue Methode, die Werthe der Integrale näherungsweise zu finden, 1826.

432 Koga, M.: Direct production of droplets from breaking wind‐waves—its observation by a multi‐
433 colored overlapping exposure photographing technique, Tellus, 33, 552-563, 1981.

434 Lhuissier, H., and Villermaux, E.: Bursting bubble aerosols, Journal of Fluid Mechanics, 696, 5-44, 2012.

435 Li, J., Waliser, D., Stephens, G., Lee, S., L'Ecuyer, T., Kato, S., Loeb, N., and Ma, H. Y.: Characterizing
436 and understanding radiation budget biases in CMIP3/CMIP5 GCMs, contemporary GCM, and reanalysis,
437 Journal of Geophysical Research: Atmospheres, 118, 8166-8184, 2013.

438 Li, J. N., and Barker, H. W.: Computation of domain‐average radiative flux profiles using Gaussian
439 quadrature, Quarterly Journal of the Royal Meteorological Society, 144, 720-734, 2018.

440 Ling, S., and Kao, T.: Parameterization of the moisture and heat transfer process over the ocean under
441 whitecap sea states, Journal of Physical Oceanography, 6, 306-315, 1976.

442 Liu, B., Guan, C., Xie, L. a., and Zhao, D.: An investigation of the effects of wave state and sea spray on
443 an idealized typhoon using an air-sea coupled modeling system, Advances in Atmospheric Sciences, 29,
444 391-406, 2012.

445 Liu, L., Zhang, C., Li, R., and Wang, B.: C-Coupler2: a flexible and user-friendly community coupler
446 for model coupling and nesting, Geoscientific Model Development Discussions, 11, 1-63,
447 http://dx.doi.org/10.5194/gmd-11-3557-2018, 2018.

448 McClarren, R.: Gauss Quadrature and Multi-dimensional Integrals, Computational Nuclear Engineering
449 and Radiological Science Using Python; Academic Press: Cambridge, MA, USA, 287-299, 2018.

450 Melville, W. K.: The role of surface-wave breaking in air-sea interaction, 1996.

451 Monahan, E., Davidson, K., and Spiel, D.: Whitecap aerosol productivity deduced from simulation tank
452 measurements, Journal of Geophysical Research: Oceans, 87, 8898-8904, 1982.

https://doi.org/10.5194/gmd-2022-233
Preprint. Discussion started: 16 November 2022

453 Monahan, E., and Van Patten, M. A.: The climate and health implications of bubble-mediated sea-air
454 exchange, 1988.
455 Praveen Kumar, B., Vialard, J., Lengaigne, M., Murty, V., and Mcphaden, M. J.: TropFlux: Air-sea
456 fluxes for the global tropical oceans—Description and evaluation, Climate dynamics, 38, 1521-1543,
457 2012.
458 Pruppacher, H. R., and Klett, J. D.: Microstructure of atmospheric clouds and precipitation, in:
459 Microphysics of Clouds and Precipitation, Springer, 9-55, 1978.
460 Resch, F., and Afeti, G.: Film drop distributions from bubbles bursting in seawater, Journal of
461 Geophysical Research: Oceans, 96, 10681-10688, 1991.
462 Reynolds, R. W., Smith, T. M., Liu, C., Chelton, D. B., Casey, K. S., and Schlax, M. G.: Daily high-
463 resolution-blended analyses for sea surface temperature, Journal of climate, 20, 5473-5496, 2007.
464 Saha, S., Moorthi, S., Wu, X., Wang, J., Nadiga, S., Tripp, P., Behringer, D., Hou, Y., Chuang, H., and
465 Iredell, M. D.: The NCEP Climate Forecast System Version 2, Journal of Climate, 27, 2185-2208,
466 http://dx.doi.org/10.1175/JCLI-D-12-00823.1, 2014.
467 Seethala, C., Zuidema, P., Edson, J., Brunke, M., Chen, G., Li, X. Y., Painemal, D., Robinson, C.,
468 Shingler, T., and Shook, M.: On assessing ERA5 and MERRA2 representations of cold‐air outbreaks
469 across the Gulf Stream, Geophysical research letters, 48, e2021GL094364, 2021.
470 Shi, R., Xu, F., Liu, L., Fan, Z., Yu, H., Li, H., Li, X., and Zhang, Y.: The effects of ocean surface waves
471 on global intraseasonal prediction: case studies with a coupled CFSv2. 0–WW3 system, Geoscientific
472 Model Development, 15, 2345-2363, 2022.
473 Smith, R. K.: On the theory of CISK, Quarterly Journal of the Royal Meteorological Society, 123, 407-
474 418, 1997.
475 Song, Y., Qiao, F., Liu, J., Shu, Q., Bao, Y., Wei, M., and Song, Z.: Effects of sea spray on large-scale
476 climatic features over the Southern Ocean, Journal of Climate, 1-51, 2022.
477 Spiel, D. E.: More on the births of jet drops from bubbles bursting on seawater surfaces, Journal of
478 Geophysical Research: Oceans, 102, 5815-5821, 1997.
479 Thorpe, S.: Bubble clouds and the dynamics of the upper ocean, Quarterly Journal of the Royal
480 Meteorological Society, 118, 1-22, 1992.

https://doi.org/10.5194/gmd-2022-233
Preprint. Discussion started: 16 November 2022

Geoscientific Model Development Discussions

481 Troitskaya, Y., Kandaurov, A., Ermakova, O., Kozlov, D., Sergeev, D., and Zilitinkevich, S.: The “bag
482 breakup” spume droplet generation mechanism at high winds. Part I: Spray generation function, Journal
483 of physical oceanography, 48, 2167-2188, 2018.
484 Van Eijk, A., Kusmierczyk‐Michulec, J., Francius, M., Tedeschi, G., Piazzola, J., Merritt, D., and
485 Fontana, J.: Sea‐spray aerosol particles generated in the surf zone, Journal of Geophysical Research:
486 Atmospheres, 116, 2011.
487 Veron, F.: Ocean spray, Annu. Rev. Fluid Mech, 47, 507-538, 2015.
488 Wallace, J. M., Mitchell, T., and Deser, C.: The influence of sea-surface temperature on surface wind in
489 the eastern equatorial Pacific: Seasonal and interannual variability, Journal of Climate, 2, 1492-1499,
490 1989.
491 Wang, C., Zhang, L., Lee, S.-K., Wu, L., and Mechoso, C. R.: A global perspective on CMIP5 climate
492 model biases, Nature Climate Change, 4, 201-205, 2014.
493 Wu, J.: Evaporation due to spray, Journal of Geophysical Research, 79, 4107-4109, 1974.
494 Wu, L., Cheng, X., Zeng, Q., Jin, J., Huang, J., and Feng, Y.: On the upward flux of sea‐spray spume
495 droplets in high‐wind conditions, Journal of Geophysical Research: Atmospheres, 122, 5976-5987,
496 2017.
497 Xu, X., Voermans, J., Liu, Q., Moon, I.-J., Guan, C., and Babanin, A.: Impacts of the Wave-Dependent
498 Sea Spray Parameterizations on Air‐Sea–Wave Coupled Modeling under an Idealized Tropical Cyclone,
499 Journal of Marine Science and Engineering, 9, 1390, 2021a.
500 Xu, X., Voermans, J., Ma, H., Guan, C., and Babanin, A. V.: A Wind–Wave-Dependent Sea Spray
501 Volume Flux Model Based on Field Experiments, Journal of Marine Science and Engineering, 9, 1168,
502 2021b.
503 Yu, L., Jin, X., and Weller, R. A.: 2008: Multidecade global flux datasets from the Objectively Analyzed
504 Air-Sea Fluxes (OAFlux) Project: Latent and sensible heat fluxes, ocean evaporation, and related surface
505 meteorological variables. Woods Hole Oceanographic Institution OAFlux Project Tec, Rep, 2008,
506 Zhao, B., Qiao, F., Cavaleri, L., Wang, G., Bertotti, L., and Liu, L.: Sensitivity of typhoon modeling to
507 surface waves and rainfall, Journal of Geophysical Research: Oceans, 122, 1702-1723, 2017.
508

https://doi.org/10.5194/gmd-2022-233
Preprint. Discussion started: 16 November 2022

Geoscientific Model Development
Discussions
Open Access
EGU

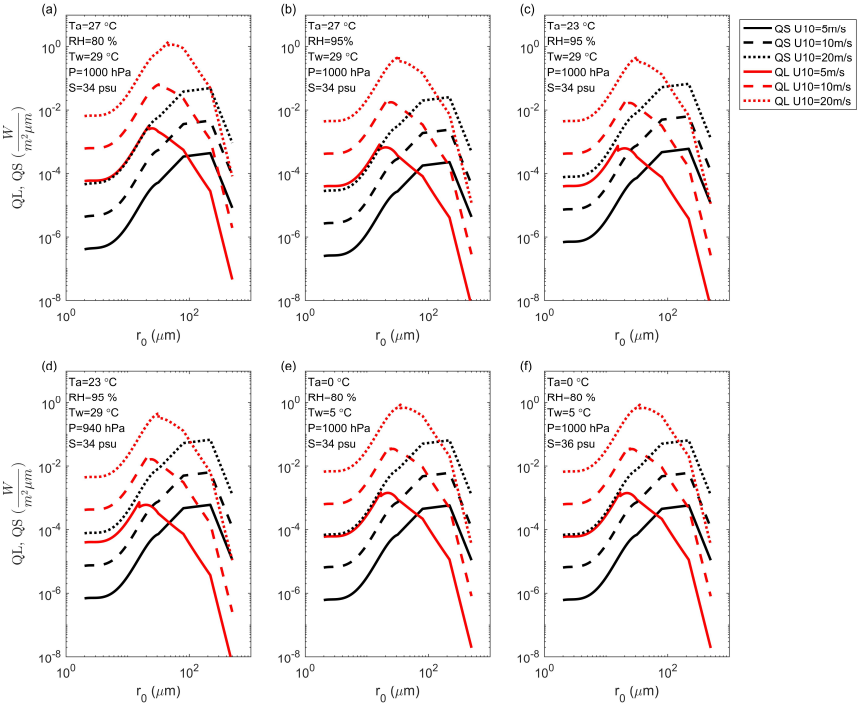

Figure 1. The radius-specific sea spray-mediated sensible (Q_S; black) and latent (Q_L; red) heat fluxes as functions of initial radius r_0: U_{10}, Ta, RH, Tw, P and S are 10-m wind speed, 2-m air temperature, 2-m relative humidity, sea surface temperature, surface air pressure and surface salinity, respectively.

https://doi.org/10.5194/gmd-2022-233
Preprint. Discussion started: 16 November 2022

Geoscientific Model Development Discussions
Open Access
EGU

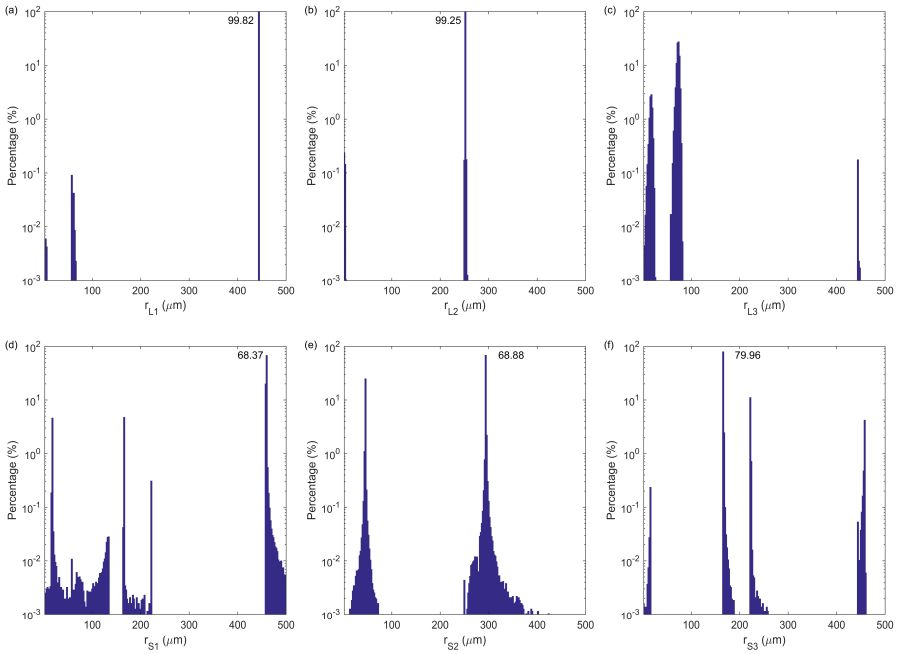

Figure 2. The distribution of occurrence frequency in percentage for GQ radius nodes: (a) the first node of latent heat flux; (b) the second node of latent heat flux; (c) the third node of latent heat flux; (d) the first node of sensible heat flux; (e) the second node of sensible heat flux; (f) the third node of sensible heat flux. The peak frequencies are marked.

https://doi.org/10.5194/gmd-2022-233
Preprint. Discussion started: 16 November 2022

Geoscientific Model Development Discussions
Open Access
EGU

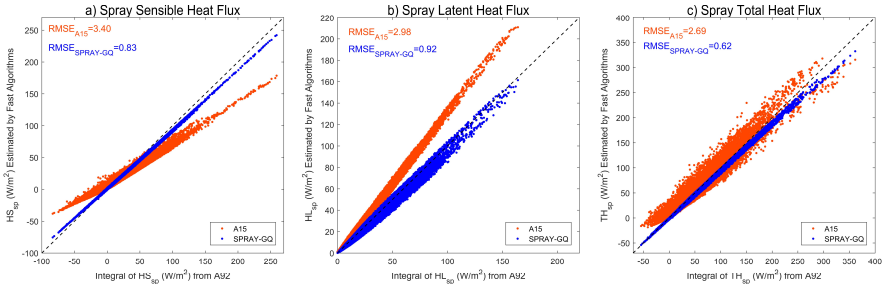

Figure 3. Scatter plots of $H_{S,SP}$ (a), $H_{L,SP}$ (b) and total heat flux $TH_{SP} = H_{S,SP}+H_{L,SP}$ (c) estimated by fast algorithms (y-axis) vs those estimated by spectral integral in microphysical parameterization (x-axis): The dotted black line is y=x. The corresponding RMSEs are marked in the upper left corner.

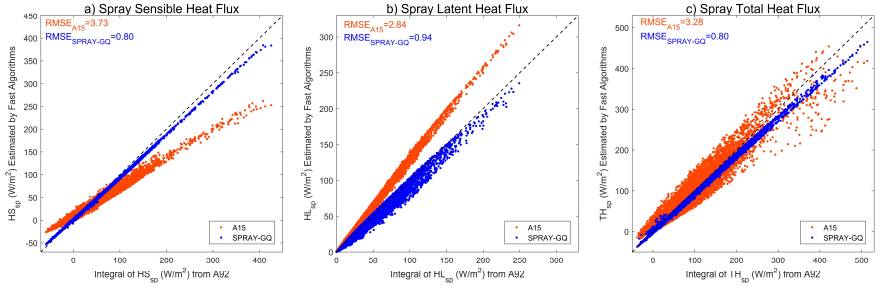

Figure 4. The same as Figure 3, but WSP10, 2-m air temperature and 2-m specific humidity of OAFlux are used.

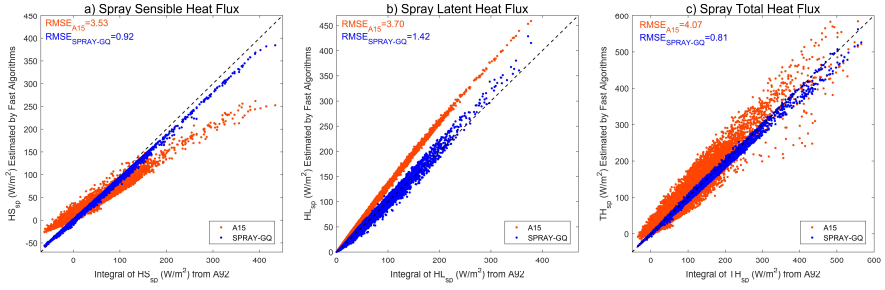

Figure 5. The same as Figure 4, but SWH are derived by WSP10 instead of ERA5 SWH.

https://doi.org/10.5194/gmd-2022-233
Preprint. Discussion started: 16 November 2022

Geoscientific Model Development Discussions
Open Access
EGU

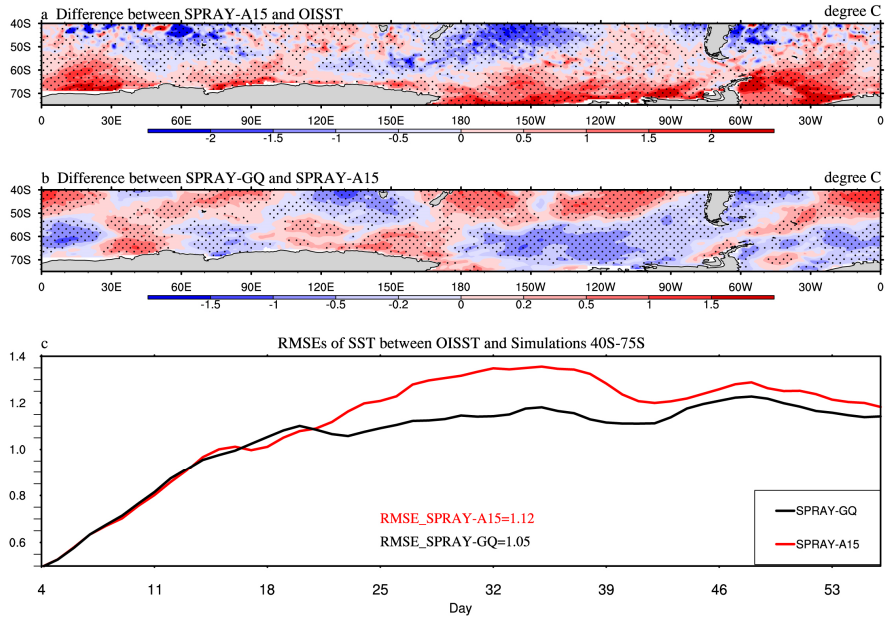

Figure 6. The 53-day average SST (°C) differences between SPRAY-A15 and OISST (a; SPRAY-A15 minus OISST), the differences between SPRAY-GQ and SPRAY-A15 (b; SPRAY-GQ minus SPRAY-A15), and the time series of domain-averaged RMSE (c; 0-360°E, 40-75°S) in Jan-Feb, 2017. The first 3-day simulation is discarded. The dotted areas are statistically significant at 95% confidence level.

https://doi.org/10.5194/gmd-2022-233
Preprint. Discussion started: 16 November 2022

Geoscientific Model Development
Discussions
Open Access
EGU

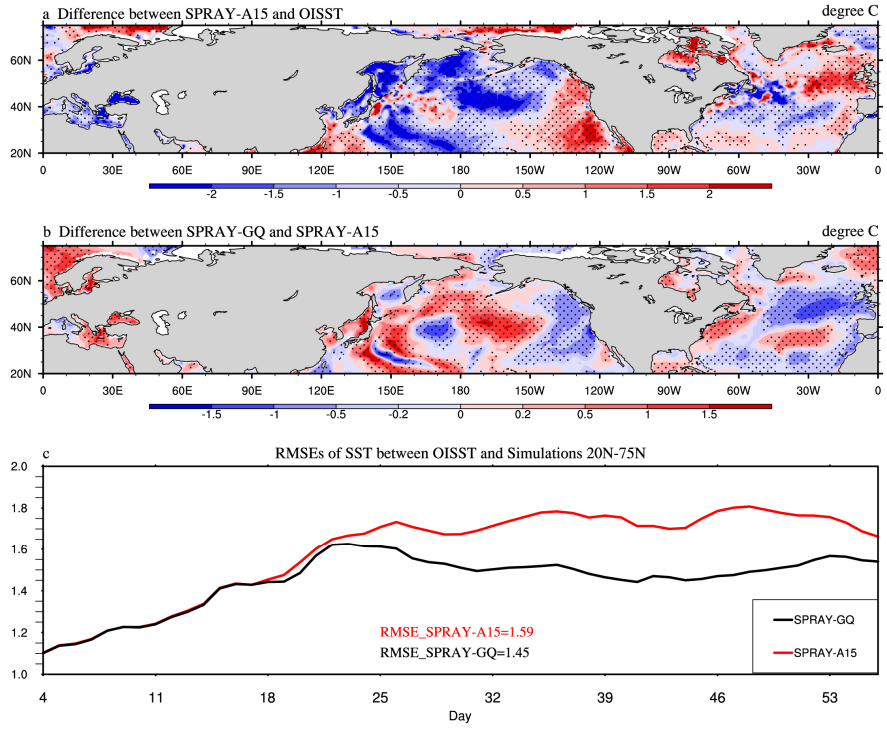

Figure 7. The same as Figure 6, but for Aug-Sep, 2018 in 0-360°E, 20-75°N.

https://doi.org/10.5194/gmd-2022-233
Preprint. Discussion started: 16 November 2022

Geoscientific Model Development Discussions
Open Access
EGU

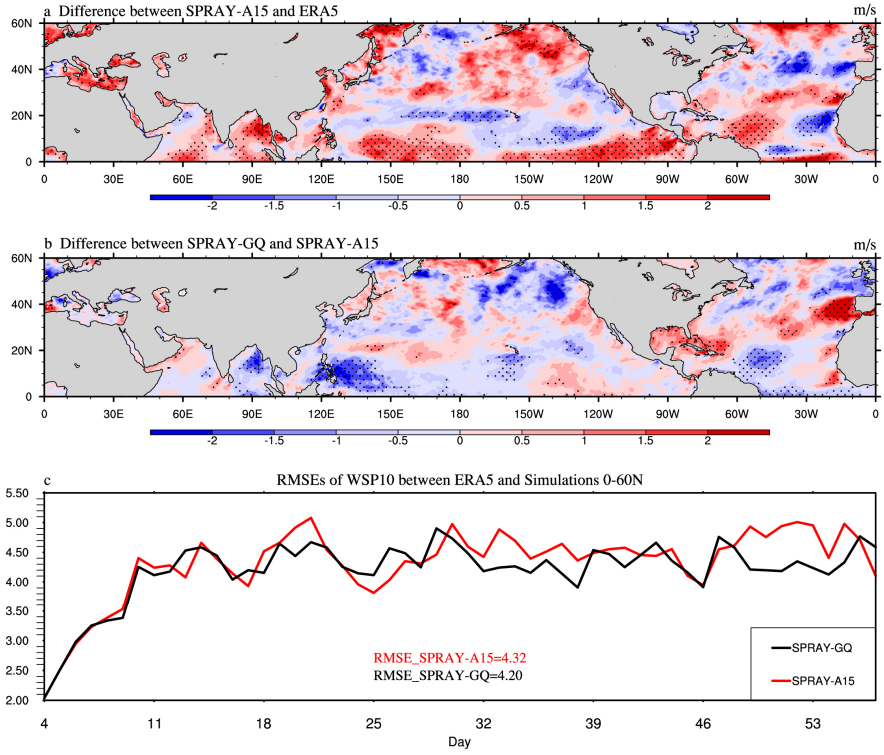

Figure 8. The 53-day average WSP10 (m/s) differences between SPRAY-A15 and ERA5 (a; SPRAY-A15 minus ERA5), the differences between SPRAY-GQ and SPRAY-A15 (b; SPRAY-GQ minus SPRAY-A15), and the time series of domain-averaged RMSE (c; 0-360°E, 0-60°N) in Jan-Feb, 2017. The first 3-day simulation is discarded. The dotted areas are statistically significant at 95% confidence level.

https://doi.org/10.5194/gmd-2022-233
Preprint. Discussion started: 16 November 2022

Geoscientific Model Development Discussions
Open Access
EGU

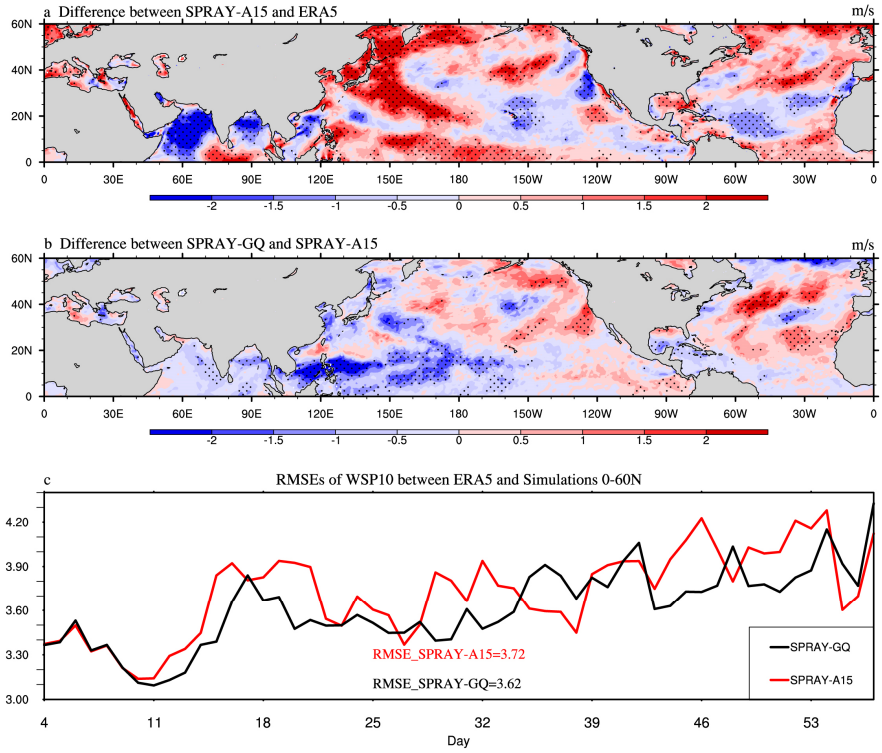

Figure 9. The same as Figure 8, but for Aug-Sep, 2018.

https://doi.org/10.5194/gmd-2022-233
Preprint. Discussion started: 16 November 2022

Geoscientific Model Development Discussions
Open Access
EGU

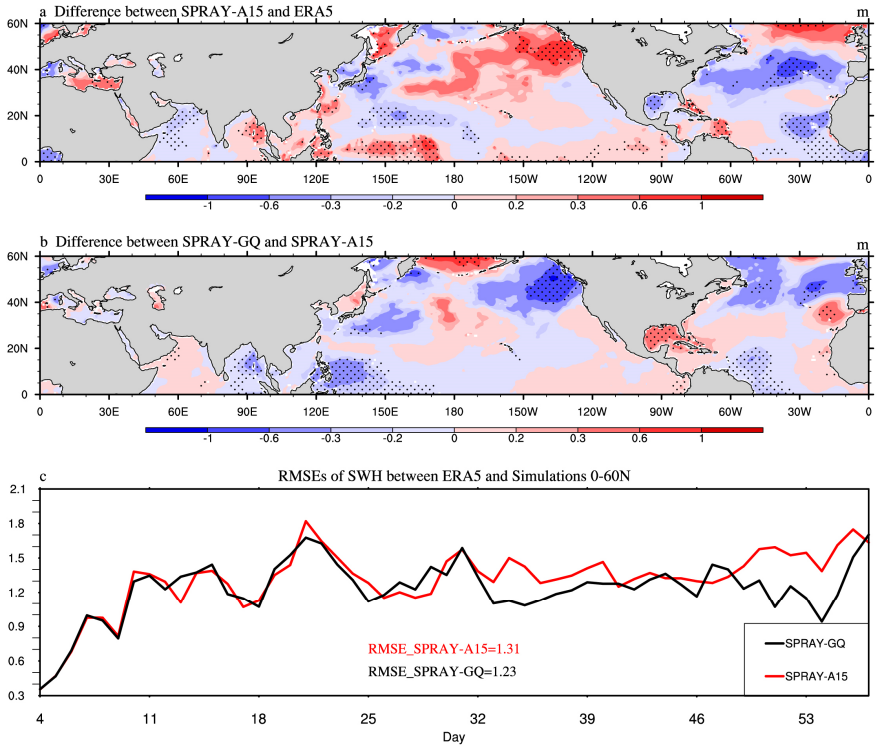

Figure 10. The 53-day average SWH (m) differences between SPRAY-A15 and ERA5 (a; SPRAY-A15 minus ERA5), the differences between SPRAY-GQ and SPRAY-A15 (b; SPRAY-GQ minus SPRAY-A15), and the time series of domain-averaged RMSE (c; 0-360°E, 0-60°N) in Jan-Feb, 2017. The first 3-day simulation is discarded. The dotted areas are statistically significant at 95% confidence level.

https://doi.org/10.5194/gmd-2022-233
Preprint. Discussion started: 16 November 2022

Geoscientific Model Development
Discussions
Open Access
EGU

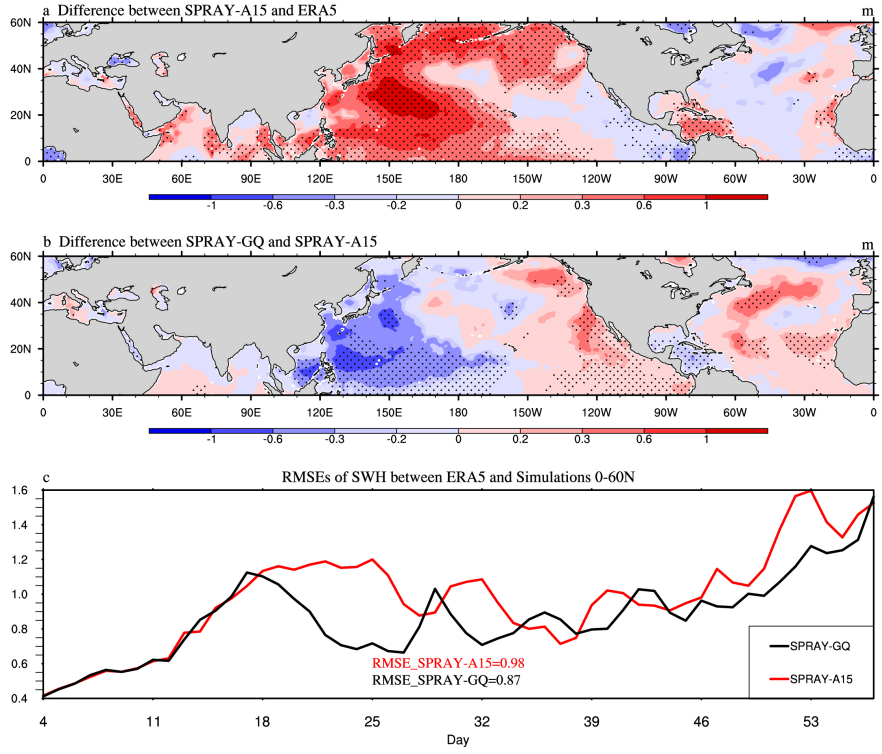

Figure 11. The same as Figure 10, but for Aug-Sep, 2018.

https://doi.org/10.5194/gmd-2022-233
Preprint. Discussion started: 16 November 2022

Geoscientific Model Development
Discussions
Open Access
EGU

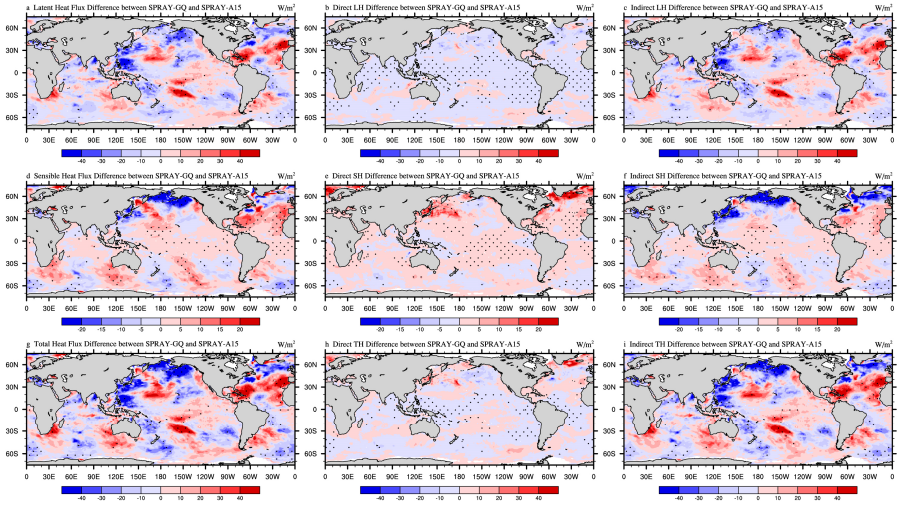

Figure 12. The 53-day average differences of latent heat flux (a-c), sensible heat flux (d-f) and total heat flux (g-i) between SPRAY-A15 and SPRAY-GQ (SPRAY-GQ minus SPRAY-A15) in Jan-Feb, 2017. The direct differences indicate sea spray-mediated heat flux differences (b, e, h), and the indirect differences indicate interfacial (bulk) heat flux differences resulted by sea spray (c, f, i). The dotted areas are statistically significant at 95% confidence level. A positive value of flux indicates an upward direction.

https://doi.org/10.5194/gmd-2022-233
Preprint. Discussion started: 16 November 2022

Geoscientific Model Development
Discussions
Open Access
EGU

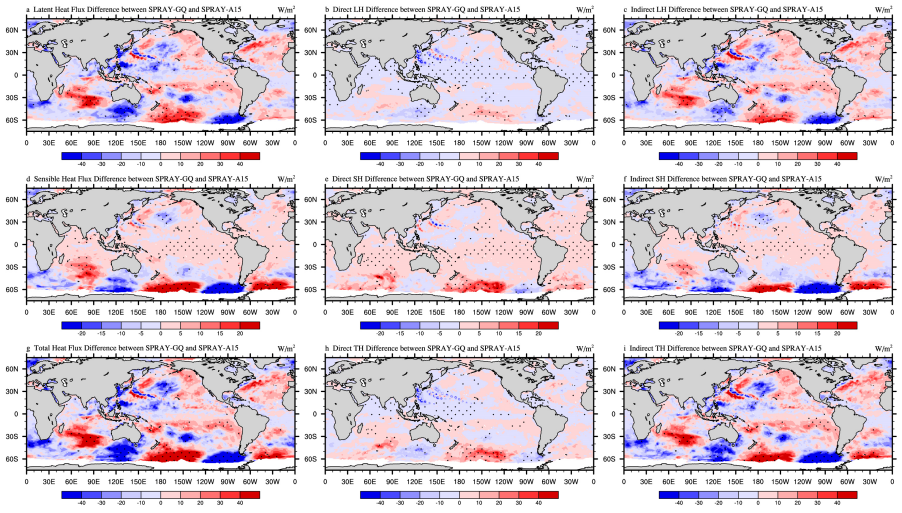

Figure 13. The same as Figure 12, but for Aug-Sep, 2018.